Letter

Ultrafast electronic linewidth broadening in the C 1*s* core level of graphene

Davide Curcio,[1] Sahar Pakdel,[1] Klara Volckaert,[1] Jill A. Miwa,[1] Søren Ulstrup,[1] Nicola Lanatà [2,3] Marco Bianchi,[1]
Dmytro Kutnyakhov,[4] Federico Pressacco,[4] Günter Brenner [4] Siarhei Dziarzhytski,[4] Harald Redlin,[4]
Steinn Ymir Agustsson [5] Katerina Medjanik,[5] Dmitry Vasilyev,[5] Hans-Joachim Elmers,[5] Gerd Schönhense,[5]
Christian Tusche,[6,7] Ying-Jiun Chen,[6,7] Florian Speck,[8] Thomas Seyller,[8] Kevin Bühlmann,[9] Rafael Gort,[9]
Florian Diekmann,[10] Kai Rossnagel,[10,11] Yves Acremann,[9] Jure Demsar,[5] Wilfried Wurth,[4,12,*] Daniel Lizzit,[13,†]
Luca Bignardi,[13,‡] Paolo Lacovig,[13] Silvano Lizzit,[13] Charlotte E. Sanders,[14] and Philip Hofmann [1]

[1]*Department of Physics and Astronomy, Interdisciplinary Nanoscience Center, Aarhus University,*
Ny Munkegade 120, 8000 Aarhus C, Denmark
[2]*Department of Physics and Astronomy, Aarhus University, 8000 Aarhus C, Denmark*
[3]*Nordita, KTH Royal Institute of Technology and Stockholm University, Roslagstullsbacken 23, 10691 Stockholm, Sweden*
[4]*Deutsches Elektronen-Synchrotron DESY, Notkestrasse 85, 22607 Hamburg, Germany*
[5]*Johannes Gutenberg-Universität, Institut für Physik, 55099 Mainz, Germany*
[6]*Peter Grünberg Institut (PGI-6), Forschungszentrum Jülich, 52425 Jülich, Germany*
[7]*Fakultät für Physik, Universität Duisburg-Essen, 47057 Duisburg, Germany*
[8]*Institut für Physik, Technische Universität Chemnitz, Reichenhainer Strasse 70, 09126 Chemnitz, Germany*
[9]*Department of Physics, Laboratory for Solid State Physics, ETH Zürich, Otto-Stern-Weg 1, 8093 Zürich, Switzerland*
[10]*Institute of Experimental and Applied Physics, Kiel University, 24098 Kiel, Germany*
[11]*Ruprecht Haensel Laboratory, Deutsches Elektronen-Synchrotron DESY, 22607 Hamburg, Germany*
[12]*Center for Free-Electron Laser Science CFEL, Hamburg University, Luruper Chausee 149, 22761 Hamburg, Germany*
[13]*Elettra-Sincrotrone Trieste S.C.p.A., Strada Statale 14 - km 163.5 in AREA Science Park, 34149 Trieste, Italy*
[14]*STFC Central Laser Facility, Research Complex at Harwell, Harwell Campus, Didcot OX11 0QX, United Kingdom*

We show that the presence of a transiently excited hot electron gas in graphene leads to a substantial broadening of the C 1*s* line probed by time-resolved x-ray photoemission spectroscopy. The broadening is found to be caused by an exchange of energy and momentum between the photoemitted core electron and the hot electron gas, rather than by vibrational excitations. This interpretation is supported by a quantitative line-shape analysis that accounts for the presence of the excited electrons. Fitting the spectra to this model directly yields the electronic temperature of the system, in good agreement with electronic temperature values obtained from valence band data. Furthermore, we show how the momentum change of the outgoing core electrons leads to a detectable but very small change in the time-resolved photoelectron diffraction pattern and to a nearly complete elimination of the core level binding energy variation associated with the presence of a narrow σ band in the C 1*s* state.

X-ray photoelectron spectroscopy (XPS) is a powerful experimental technique for chemical analysis. It also gives detailed information on element- and site-specific many-body effects via the photoemission line shape [1]. The only temperature dependence usually considered in the XPS line shape is Gaussian broadening due to phonon excitation at high temperatures. However, it has been predicted almost 40 years ago that excited electron-hole pairs could affect the XPS linewidth and line shape for high (electronic) temperatures [2]. This has yet to be confirmed, presumably because such electronic effects are masked by vibrational broadening at high sample temperatures.

The advent of ultrafast pump-probe XPS at free electron laser (FEL) sources now offers the opportunity to separate electronic and vibrational contributions to the XPS line shape since either the electronic or specific vibrational degrees of freedom can be addressed by choosing an appropriate pump energy [3,4]. While high-resolution line-shape studies are challenging at FELs due to the low repetition rate and the presence of space charge effects [5–9], a detailed XPS line-shape investigation has recently been presented for pumped WSe_2, tracking an excitonic Mott transition [10].

Here, we study the ultrafast evolution of the C 1*s* line shape, intensity, and binding energy in graphene upon pumping the electronic system to high temperatures. After the

*Deceased.
†Present address: Polytechnic Department of Engineering and Architecture (DPIA), University of Udine, 33100 Udine, Italy.
‡Present address: Department of Physics, University of Trieste, Via Valerio 2, 34127 Trieste, Italy.
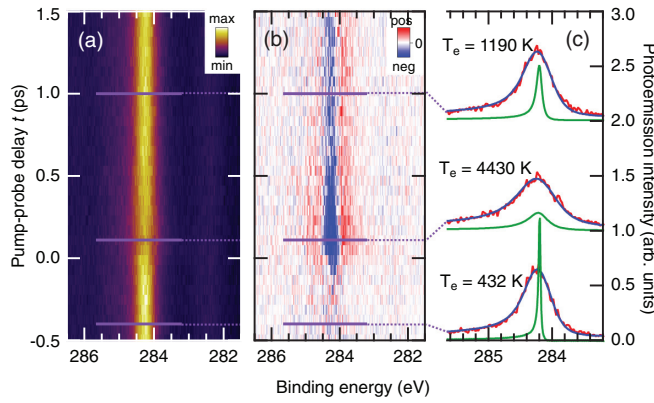
FIG. 1. (a) C 1*s* photoemission intensity as a function of pump-probe delay and binding energy. (b) Same as in (a) but with the average spectrum before excitation subtracted. Red and blue indicate an increase and decrease in electron counts, respectively. (c) Selected spectra (cuts at specific time delays) along with best fit to the model described in the text (blue line). The temperature-dependent asymmetry kernel for each fit is shown in green. The electronic temperatures resulting from the fit are noted close to the spectra.

excitation with an infrared pump pulse, the electrons thermalize within a few tens of fs. The hot electron gas in the Dirac cone of graphene initially experiences a rapid energy loss via strongly coupled optical phonons but cooling quickly ceases to be efficient due to several bottlenecks for energy dissipation processes [11–20]. This opens the possibility of studying the effect of a hot electron gas on the core level spectrum while the lattice remains essentially at equilibrium, at least within the first stages of the excitation.

We performed time- and angle-resolved XPS and valence band photoemission experiments on the momentum microscope-based setup at the PG2 beamline of FLASH [21], using hydrogen-intercalated quasi-free-standing monolayer graphene on SiC [22,23]. The pump photon energy and fluence were 1.55 eV and ≈ 0.5 mJ cm^{-2}, respectively. The probe photon energies were 337.5 and 112.5 eV for the C 1*s* data and the valence band, respectively. For other experimental details, see the Supplemental Material (SM) [24] (see also Refs. [25–35] therein).

Figures 1(a)–1(c) show the time-dependent graphene C 1*s* core level intensity as a function of binding energy and pump-probe time delay *t*, the difference between the time-dependent photoemission intensity and the average spectrum before the excitation, and spectra at selected time delays. The pump-induced excitation of graphene around $t = 0$ is clearly reflected in a broadening of this peak. The pump-induced broadening is a large effect: It increases the C 1*s* linewidth by almost 280 meV, from 560 to 840 meV at peak excitation, recovering to 580 meV in our measured pump-probe delay window.

In order to quantify the pump-induced line-shape changes, we modify a model for the core level photoemission intensity proposed by Hughes and Scarfe [36]. Their expression for the energy-dependent photoemission intensity $I(E)$ of a core level

at energy E_0 is

$$I(E) \propto \int_{-\infty}^{+\infty} e^{-iEt} e^{-iE_0 t} e^{-\lambda|t|} e^{-\frac{\sigma^2 t^2}{2}}$$
$$\times \exp\left(\int_0^{+\infty} J(E') \frac{e^{iE't} - 1}{E'^2} dE'\right) dt, \quad (1)$$

where λ sets the Lorentzian width describing the lifetime broadening and σ sets the Gaussian width that includes the effects of phonon broadening and experimental energy resolution. The last integral in the exponential describes the possible low-energy energy losses during the photoemission process, such as the electron-hole excitations in metals. $J(E')$ encodes the density of possible excitations in the zero temperature limit. This general line-shape model includes the asymmetric Doniach-Šunjić line shape as a special case and it provides a good description of static XPS from graphene [22,37]. However, it is not appropriate for high electronic temperatures because of two effects: (1) Given the substantial population of states above E_F, the possible excitation of electrons in the photoemission process is no longer restricted to electrons below E_F, and (2) the outgoing electron may not only lose energy by exciting an electron-hole pair, but also *gain* energy upon electron-hole recombination [2]. We include these finite temperature effects by setting the lower integration limit in the last integral of Eq. (1) to $-\infty$ in order to also allow for energy gains. We further define a finite temperature version of $J(E')$,

$$J(E') = a^2 \int_{-\infty}^{+\infty} D(\epsilon) f(\epsilon, T_e) D(\epsilon + E')$$
$$\times [1 - f(\epsilon + E', T_e)] d\epsilon, \quad (2)$$

where $D(\epsilon)$ is the density of states, T_e is the electronic temperature, and $f(\epsilon, T_e)$ the Fermi-Dirac distribution.

The fit to the data in Fig. 1 is performed by fixing λ and a obtained from the un-pumped data in order to minimize space charge effects, σ and E_0 from data at negative time delays, and using the electronic temperature T_e as the only line-shape fit parameter for the entire series of pumped data. The density of states $D(\epsilon)$ is taken to be constant [24]. The simple model leads to an excellent fit to the data, as shown for the example spectra in Fig. 1(c). We not only show the actual fit but also the temperature-dependent asymmetry kernel [shifted by E_0, green curves in Fig. 1(c)], which is the Fourier transform of the last term in Eq. (1). For the unpumped system, the asymmetry kernel is strongly peaked and its intensity is largely found at energies higher than the peak binding energy, giving rise to the characteristic asymmetric line shape. This is expected because the inelastic processes are completely dominated by energy losses. At peak excitation, on the other hand, the electronic temperature reaches 4200 K and the asymmetry kernel is much broader. Also, its median moves to a lower binding energy, emphasizing the contribution of processes involving an energy gain.

Figure 2 shows the time-dependent electronic temperature resulting from the fit. It is qualitatively similar to previous experimental [14,15] and theoretical [20] results from the same system, and also to the electronic temperature directly obtained from the Fermi-Dirac distribution in the valence band, using the approach outlined in Refs. [15,38] (gray line
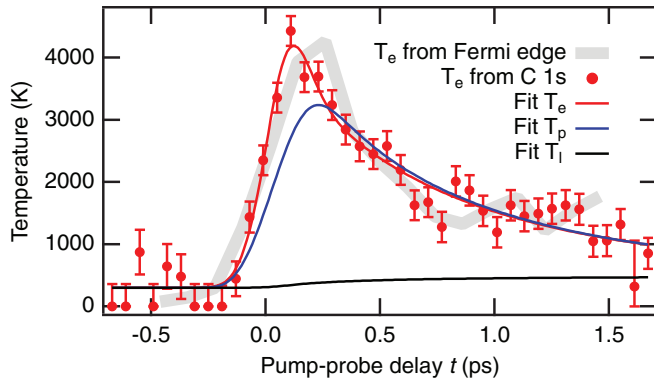
FIG. 2. Time-dependent electronic temperature extracted from the fit of the C 1s core level data in Fig. 1(a) (red markers). The red solid line is a fit to the electronic temperature T_e using a three-temperature model, giving the temperatures of the strongly coupled phonons T_p (blue line) and the remaining lattice T_l (black line). The gray, thick line corresponds to the T_e obtained from an analysis of the Fermi-Dirac distribution in the valence band.

in Fig. 2). The electronic temperature after excitation obtained from the core level data is well described by a double exponential decay with time constants of $\tau_1 = 170(50)$ fs and $\tau_2 = 1.3(2)$ ps, also similar to literature values [14,15,17].

For a more detailed analysis, we fit the electronic temperature from the C 1s spectra using the three-temperature model described in Ref. [15]. This yields a good fit to T_e, along with the time-dependent temperatures of the strongly coupled optical phonons (T_p) and the acoustic phonon bath (T_l). The result of this fit is also shown in Fig. 2. The coupling constants we find are $\lambda_1 = 0.06(4)$ (coupling to strongly coupled optical phonons) and $\lambda_2 = 0.0029(6)$ (coupling to acoustic phonons), similar to what has been reported for lightly doped graphene [15,39,40].

Electronic broadening is completely sufficient to describe the C 1s line-shape changes and conventional phonon broadening appears to be insignificant. This is confirmed if we multiply the intrinsic low-temperature Gaussian contribution to the linewidth of ≈ 110 meV [41] by the statistical Bose-Einstein broadening factor for a ≈ 200 meV phonon at $T_p = 3200$ K, giving rise to a total linewidth of less than 190 meV [1]. We can also extrapolate the measured temperature-dependent linewidth from equilibrium XPS data in Ref. [41] to 3200 K, resulting in less than 400 meV. This strongly overestimates the broadening expected for a high T_p because it corresponds to a situation in which *all* phonons are excited to 3200 K. Still, the resulting broadening is much smaller than the one observed here.

We now explore the effect of the strong electronic final state scattering on the **k**-resolved photoemission intensity and core level binding energy. Figure 3(a) shows the C 1s core level intensity, integrated over the time interval before the arrival of the pump pulse. The data are displayed in terms of a so-called modulation function χ, a quantity commonly used in x-ray photoelectron diffraction (XPD) [24,42]. Intensity modulations arise from the interference between the part of the electron wave field reaching the detector directly and the parts that are elastically scattered by the atoms surrounding
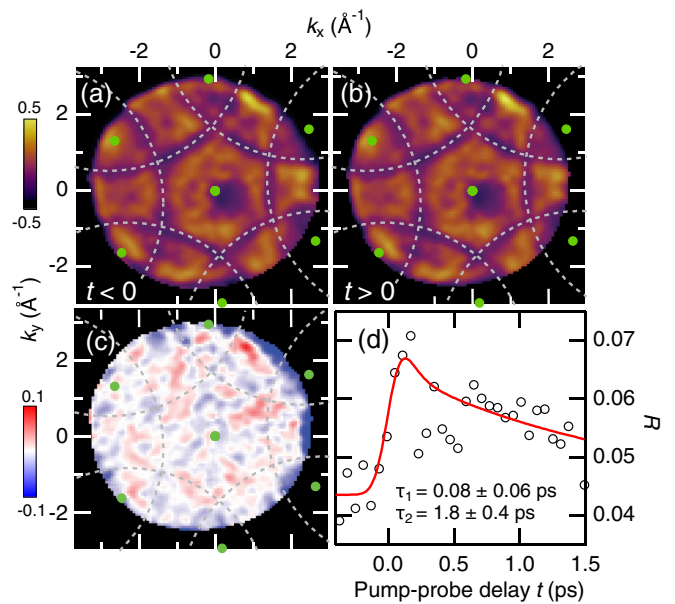
FIG. 3. (a) C 1s photoemission intensity integrated over negative pump-probe delay times, displayed as a modulation function in momentum space. The Γ points are shown in green. The dashed lines emphasize regions of low photoemission intensity ("dark lines") arising from a combination of scattering by the graphene reciprocal lattice and reflection at the surface potential. (b) The same as in (a), but integrated over positive time delays. (c) Difference of the modulation functions in (a) and (b). (d) Comparison between the time-dependent modulation function and the equilibrium modulation function, quantified by $R(t)$. A fit to the data using a double decaying exponential convoluted with a Gaussian is shown in red.

the emitting carbon atom. Such modulations can be used for a local structural determination [24,37,42]. In addition to the scattering-induced XPD features, χ contains a dominant contribution from the curved "dark lines" emphasized by dashed lines. These are due to an interference effect involving scattering by the graphene reciprocal lattice combined with reflection at the surface potential boundary [43].

We can probe the effect of ultrafast electronic final state excitations on the XPD pattern by comparing the XPD patterns after excitation to those at equilibrium [44,45]. To this end, Fig. 3(b) shows the modulation function integrated over the positive time delays between 0 and 1.5 ps and Fig. 3(c) gives the difference between Figs. 3(a) and 3(b). Clearly, the excitation-induced changes are very small such that Fig. 3(c) represents largely noise. From a mere inspection of these data, we can conclude that the electronic final state line-shape broadening does not preclude a time-dependent structural determination by XPD.

A more quantitative analysis of the XPD pattern's time evolution can be performed by introducing $R(t) = \sum_i [\chi_i - \chi_i(t)]^2 / \sum_i [\chi_i^2 + \chi_i(t)^2]$, where χ and $\chi(t)$ are the modulation functions at equilibrium and delay time t, respectively, and the sum runs over all the points in the diffraction pattern. The resulting $R(t)$ is shown in Fig. 3(d). As expected, the time-dependent variation of $R(t)$ is very small. Surprisingly though, a signature of the pump-induced excitation is still clearly visible and despite the uncertainties resulting from

inspecting the very small changes in $R(t)$, its time dependence is similar to that of the electronic temperature. To see this, we fit $R(t)$ to the same double exponential decay model as used for core level data, resulting in consistent time constants of $\tau_1' = 0.08(6)$ ps and $\tau_2' = 1.8(4)$ ps. Note that structural changes are not expected to influence $R(t)$ because of the small increase of T_l. Also, an anharmonic change of the average lattice constant can be ruled out by the fact that the position of the dark lines in the diffraction pattern, and thus the size of the reciprocal lattice vectors, remains fixed.

The mechanism for an electronic change of the XPD pattern is essentially the same as that leading to the line-shape change in Fig. 1: The inelastic electron-hole generation (annihilation) process giving rise to an energy loss (gain) of the photoelectron is necessarily accompanied by a momentum change. In lightly doped graphene, there are strong constraints on such momentum changes: Electron-hole pair creation or annihilation can proceed within a given Dirac cone (intravalley) or between Dirac cones (intervalley). The latter process is usually insignificant for carrier scattering in transport because it requires a strongly localized potential scatterer [46]. In our case it can be important because of the localized character of core hole generation. The momentum change in the electron-hole pair creation/annihilation process leading to the line broadening in Fig. 1 is thus approximately either zero for intravalley, or K-K' for intervalley processes. An additional momentum change corresponding to a reciprocal lattice vector is also possible. The similar time dependence of $R(t)$ and T_e suggests that the same momentum changes are responsible for the changes of the XPS line shape and the XPD pattern.

Given the importance of inelastic scattering in the line-shape change in Fig. 1 and the fact that the momentum changes can be large, it appears surprising that the XPD pattern changes so little. Qualitatively, this can be understood as follows: If a core electron escapes leaving behind an excited electron-hole pair, the momentum change deflects the primary emitted electron and it thereby changes the angular distribution of the primary electron's wave field reaching the detector and the surrounding scatterers. However, it does *not* affect the location of the scatterers relative to the emitter. Therefore, the phase difference between the part of the wave field reaching the detector directly and the scattered parts remains fixed and so does the location of the XPD features. Only the relative amplitude of the direct and scattered waves changes, modifying the intensity of the XPD features. Using simulated diffraction patterns, it can be shown that the observed change of $R(t)$ is consistent with a situation in which a substantial number (50%) of the photoelectrons have been deflected in momentum because of the creation/annihilation of electron-hole pairs in the photoemission process [24].

Graphene offers the unique possibility to further test the role of electronic final state scattering in the C 1s spectrum due to the fact that the C 1s state forms a narrow σ band with a splitting between bonding and antibonding states of 60 meV at the Γ point [37] [see Fig. S5(a) in the SM [24]]. The splitting is too small to be directly observable given the natural C 1s linewidth but, due to the selection rules in the bipartite graphene lattice [47,48], only the bonding band is visible in the first Brillouin zone (BZ), whereas mainly the antibonding band is visible in the neighboring zones. This dominance
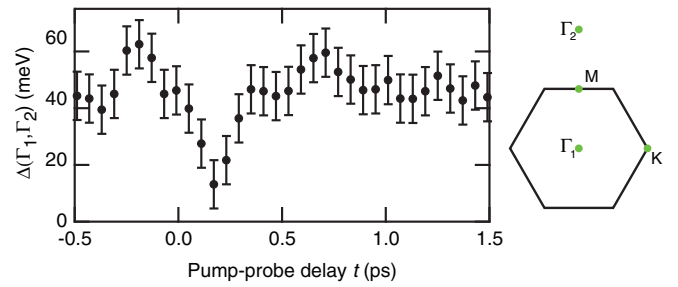
FIG. 4. Time-dependent C 1s bandwidth obtained from the energy difference between the C 1s peaks at the Γ_1 and Γ_2 points of the first and the neighboring Brillouin zone (see sketch on the right-hand side).

of one particular band makes the dispersion observable as a slight shift of the C 1s peak between the Γ points of different BZs, e.g., between Γ_1 and Γ_2 in the sketch of Fig. 4 [37].

We can exploit this effect for confirming the presence of inelastic momentum deflection in the electronic final state. When explaining the ultrafast changes of the XPD pattern in Fig. 3, we have argued that the inelastic excitation/annihilation of electron-hole pairs during the photoemission process is accompanied by a momentum change of the photoelectron which is either zero or K-K' modulo a reciprocal lattice vector. Here, we immediately notice that momentum changes involving a reciprocal lattice vector could completely eliminate the observed binding energy difference between the Γ_1 and Γ_2 points, $\Delta(\Gamma_1, \Gamma_2)$. Even changes involving a momentum change of K-K', which is the same scattering vector as Γ-K, could greatly reduce $\Delta(\Gamma_1, \Gamma_2)$ since they mix electrons from the K points, where there is no energy difference between bonding and antibonding band, into the Γ points. If electronic scattering effects are indeed important, the dispersion of the σ band might no longer be observable.

This is indeed seen when plotting the time-dependent energy difference $\Delta(\Gamma_1, \Gamma_2)$ in Fig. 4. Upon pumping the system, $\Delta(\Gamma_1, \Gamma_2)$ reduces from around 45 meV to roughly 10 meV on a similar timescale as the electronic temperature change. This is followed by a recovery to the equilibrium levels that is more swift than the T_e recovery, which could be explained by a nonlinear relationship between T_e and the measured $\Delta(\Gamma_1, \Gamma_2)$. A quantitative estimate of the effect is presented in the SM [24]. Assuming that half of the emitted electrons are inelastically deflected turns out to be sufficient to reduce $\Delta(\Gamma_1, \Gamma_2)$ from 45 to 10 meV, similar to what is observed in the experiment. This scenario is also consistent with the minor change of the XPD pattern reported in Fig. 3.

In conclusion, we have demonstrated the potential of high-resolution time-resolved XPS to give detailed information on the ultrafast development of electronic many-body effects. In particular, we have identified an electronic broadening mechanism in which the outgoing core level electron exchanges energy and momentum with the hot electron gas. This interpretation of the data is supported by an ultrafast suppression of the momentum-dependent binding energy variations associated with the C 1s σ band. Moreover, a

quantitative description of the resulting line shape permits the determination of the electronic temperature in agreement with direct measurements in the valence band. It will be interesting to expand the technique to very short time delays, before the thermalization of the electron gas, where high-resolution XPS will provide an element-specific probe of the electronic excitations and many-body effects. The ultrafast electronic final state scattering effect observed here could, in principle, impose some severe limitations for techniques such as ultrafast XPD because it could be expected to smear out the diffraction pattern. We demonstrate that this is not the case and that the XPD pattern shows only very minor changes, even at electronic temperatures of over 4000 K.

[1] P. H. Citrin, G. K. Wertheim, and Y. Baer, Phys. Rev. B **16**, 4256 (1977).

[2] S. Satpathy and J. D. Dow, Solid State Commun. **42**, 637 (1982).

[3] A. de la Torre, D. M. Kennes, M. Claassen, S. Gerber, J. W. McIver, and M. A. Sentef, arXiv:2103.14888.

[4] A. Zong, A. Kogar, and N. Gedik, MRS Bulletin **46**, 720 (2021).

[5] S. Passlack, S. Mathias, O. Andreyev, D. Mittnacht, M. Aeschlimann, and M. Bauer, J. Appl. Phys. **100**, 024912 (2006).

[6] A. Pietzsch, A. Föhlisch, M. Beye, M. Deppe, F. Hennies, M. Nagasono, E. Suljoti, W. Wurth, C. Gahl, K. Döbrich, and A. Melnikov, New J. Phys. **10**, 033004 (2008).

[7] S. Hellmann, K. Rossnagel, M. Marczynski-Bühlow, and L. Kipp, Phys. Rev. B **79**, 035402 (2009).

[8] S. Hellmann, C. Sohrt, M. Beye, T. Rohwer, F. Sorgenfrei, M. Marczynski-Bühlow, M. Kalläne, H. Redlin, F. Hennies, M. Bauer, and K. Rossnagel, New J. Phys. **14**, 013062 (2012).

[9] G. Schönhense, D. Kutnyakhov, F. Pressacco, M. Heber, N. Wind, S. Y. Agustsson, S. Babenkov, D. Vasilyev, O. Fedchenko, S. Chernov, L. Rettig, B. Schönhense, L. Wenthaus, G. Brenner, S. Dziarzhytski, S. Palutke, S. K. Mahatha, N. Schirmel, H. Redlin, B. Manschwetus *et al.*, Rev. Sci. Instrum. **92**, 053703 (2021).

[10] M. Dendzik, R. P. Xian, E. Perfetto, D. Sangalli, D. Kutnyakhov, S. Dong, S. Beaulieu, T. Pincelli, F. Pressacco, D. Curcio, S. Y. Agustsson, M. Heber, J. Hauer, W. Wurth, G. Brenner, Y. Acremann, P. Hofmann, M. Wolf, A. Marini, G. Stefanucci *et al.*, Phys. Rev. Lett. **125**, 096401 (2020).

[11] S. Butscher, F. Milde, M. Hirtschulz, E. Malic, and A. Knorr, Appl. Phys. Lett. **91**, 203103 (2007).

[12] W.-K. Tse and S. Das Sarma, Phys. Rev. B **79**, 235406 (2009).

[13] H. Wang, J. H. Strait, P. A. George, S. Shivaraman, V. B. Shields, M. Chandrashekhar, J. Hwang, F. Rana, M. G. Spencer, C. S. Ruiz-Vargas, and J. Park, Appl. Phys. Lett. **96**, 081917 (2010).

[14] I. Gierz, J. C. Petersen, M. Mitrano, C. Cacho, I. C. E. Turcu, E. Springate, A. Stöhr, A. Köhler, U. Starke, and A. Cavalleri, Nat. Mater. **12**, 1119 (2013).

[15] J. C. Johannsen, S. Ulstrup, F. Cilento, A. Crepaldi, M. Zacchigna, C. Cacho, I. C. E. Turcu, E. Springate, F. Fromm, C. Raidel, T. Seyller, F. Parmigiani, M. Grioni, and P. Hofmann, Phys. Rev. Lett. **111**, 027403 (2013).

[16] M. Sentef, A. F. Kemper, B. Moritz, J. K. Freericks, Z.-X. Shen, and T. P. Devereaux, Phys. Rev. X **3**, 041033 (2013).

[17] J. C. Johannsen, S. Ulstrup, A. Crepaldi, F. Cilento, M. Zacchigna, J. A. Miwa, C. Cacho, R. T. Chapman, E. Springate, F. Fromm, C. Raidel, T. Seyller, P. D. King, F. Parmigiani, M. Grioni, and P. Hofmann, Nano Lett. **15**, 326 (2015).

[18] S. Aeschlimann, R. Krause, M. Chávez-Cervantes, H. Bromberger, R. Jago, E. Malić, A. Al-Temimy, C. Coletti, A. Cavalleri, and I. Gierz, Phys. Rev. B **96**, 020301(R) (2017).

[19] G. Rohde, A. Stange, A. Müller, M. Behrendt, L.-P. Oloff, K. Hanff, T. J. Albert, P. Hein, K. Rossnagel, and M. Bauer, Phys. Rev. Lett. **121** 256401 (2018).

[20] F. Caruso, D. Novko, and C. Draxl, Phys. Rev. B **101**, 035128 (2020).

[21] D. Kutnyakhov, R. P. Xian, M. Dendzik, M. Heber, F. Pressacco, S. Y. Agustsson, L. Wenthaus, H. Meyer, S. Gieschen, G. Mercurio, A. Benz, K. Bühlman, S. Däster, R. Gort, D. Curcio, K. Volckaert, M. Bianchi, C. Sanders, J. A. Miwa, S. Ulstrup *et al.*, Rev. Sci. Instrum. **91**, 013109 (2020).

[22] C. Riedl, C. Coletti, T. Iwasaki, A. A. Zakharov, and U. Starke, Phys. Rev. Lett. **103**, 246804 (2009).

[23] F. Speck, J. Jobst, F. Fromm, M. Ostler, D. Waldmann, M. Hundhausen, H. B. Weber, and T. Seyller, Appl. Phys. Lett. **99**, 122106 (2011).

[24] See Supplemental Material at http://link.aps.org/supplemental/10.1103/PhysRevB.104.L161104 for details on the experimental conditions, data preparation, the C 1*s* line shape for

quasi-free-standing graphene on SiC, models for $D(\epsilon)$, the R factor, the multiple scattering simulations, the effect of the inelastic electron-hole pair generation/annihilation on $R(T)$, a quantitative theoretical estimation of $\Delta(\Gamma_1, \Gamma_2)$, the time-dependent C $1s$ binding energy at the M points, a frozen-phonon model for the initial state dispersion of C $1s$, as well as a GW calculation of the temperature-dependent C $1s$ band structure, which includes Refs. [25–35].

[25] R. P. Xian, Y. Acremann, S. Y. Agustsson, M. Dendzik, K. Bühlmann, D. Curcio, D. Kutnyakhov, F. Pressacco, M. Heber, S. Dong, T. Pincelli, J. Demsar, W. Wurth, P. Hofmann, M. Wolf, M. Scheidgen, L. Rettig, and R. Ernstorfer, Sci. Data **7**, 442 (2020).

[26] M. Keunecke, M. Reutzel, D. Schmitt, A. Osterkorn, T. A. Mishra, C. Möller, W. Bennecke, G. S. M. Jansen, D. Steil, S. R. Manmana, S. Steil, S. Kehrein, and S. Mathias, Phys. Rev. B **102**, 161403(R) (2020).

[27] A. Abrami, M. Barnaba, L. Battistello, A. Bianco, B. Brena, G. Cautero, Q. H. Chen, D. Cocco, G. Comelli, S. Contrino, F. DeBona, S. Di Fonzo, C. Fava, P. Finetti, P. Furlan, A. Galimberti, A. Gambitta, D. Giuressi, R. Godnig, W. Jark *et al.*, Rev. Sci. Instrum. **66**, 1618 (1995).

[28] B. Schönhense, K. Medjanik, O. Fedchenko, S. Chernov, M. Ellguth, D. Vasilyev, A. Oelsner, J. Viefhaus, D. Kutnyakhov, W. Wurth, H. J. Elmers, and G. Schönhense, New J. Phys. **20**, 033004 (2018).

[29] C. Coletti, K. V. Emtsev, A. A. Zakharov, T. Ouisse, D. Chaussende, and U. Starke, Appl. Phys. Lett. **99**, 081904 (2011).

[30] B. E. Sernelius, Phys. Rev. B **91**, 045402 (2015).

[31] D. P. Woodruff and A. M. Bradshaw, Rep. Prog. Phys. **57**, 1029 (1994).

[32] F. J. García de Abajo, M. A. Van Hove, and C. S. Fadley, Phys. Rev. B **63**, 075404 (2001).

[33] R. Dovesi, R. Orlando, A. Erba, C. M. Zicovich-Wilson, B. Civalleri, S. Casassa, L. Maschio, M. Ferrabone, M. De La

Pierre, P. D'Arco *et al.*, Int. J. Quantum Chem. **114**, 1287 (2014).

[34] S. Moser, J. Electron Spectrosc. Relat. Phenom. **214**, 29 (2017).

[35] J. P. Perdew, K. Burke, and M. Ernzerhof, Phys. Rev. Lett. **77**, 3865 (1996).

[36] H. P. Hughes and J. A. Scarfe, J. Phys.: Condens. Matter **8**, 1421 (1996).

[37] S. Lizzit, G. Zampieri, L. Petaccia, R. Larciprete, P. Lacovig, E. D. L. Rienks, G. Bihlmayer, A. Baraldi, and P. Hofmann, Nat. Phys. **6**, 345 (2010).

[38] S. Ulstrup, J. C. Johannsen, M. Grioni, and P. Hofmann, Rev. Sci. Instrum. **85**, 013907 (2014).

[39] S. Ulstrup, M. Bianchi, R. Hatch, D. Guan, A. Baraldi, D. Alfè, L. Hornekær, and P. Hofmann, Phys. Rev. B **86**, 161402(R) (2012).

[40] M. Calandra and F. Mauri, Phys. Rev. B **76**, 205411 (2007).

[41] M. Pozzo, D. Alfè, P. Lacovig, P. Hofmann, S. Lizzit, and A. Baraldi, Phys. Rev. Lett. **106**, 135501 (2011).

[42] D. Woodruff, J. Electron Spectrosc. Relat. Phenom. **126**, 55 (2002).

[43] A. Winkelmann, M. Ellguth, C. Tusche, A. A. Ünal, J. Henk, and J. Kirschner, Phys. Rev. B **86**, 085427 (2012).

[44] M. Greif, L. Kasmi, L. Castiglioni, M. Lucchini, L. Gallmann, U. Keller, J. Osterwalder, and M. Hengsberger, Phys. Rev. B **94**, 054309 (2016).

[45] A. K. R. Ang, Y. Fukatsu, K. Kimura, Y. Yamamoto, T. Yonezawa, H. Nitta, A. Fleurence, S. Yamamoto, I. Matsuda, Y. Yamada-Takamura, and K. Hayashi, Jpn. J. Appl. Phys. **59**, 100902 (2020).

[46] S. Das Sarma, S. Adam, E. H. Hwang, and E. Rossi, Rev. Mod. Phys. **83**, 407 (2011).

[47] E. L. Shirley, L. J. Terminello, A. Santoni, and F. J. Himpsel, Phys. Rev. B **51**, 13614 (1995).

[48] M. Mucha-Kruczynski, O. Tsyplyatyev, A. Grishin, E. McCann, V. I. Fal'ko, A. Bostwick, and E. Rotenberg, Phys. Rev. B **77**, 195403 (2008).